Journal of Zhejiang University-SCIENCE B (Biomedicine & Biotechnology)
ISSN 1673-1581 (Print); ISSN 1862-1783 (Online)
www.jzus.zju.edu.cn; www.springerlink.com
E-mail: jzus@zju.edu.cn

Mitochondrial superoxide anions induced by exogenous oxidative stress determine tumor cell fate: an individual cell-based study*

Hui PAN[†§1], Bao-hui WANG[†§2], Zhou-bin LI[1], Xing-guo GONG[3], Yong QIN[3], Yan JIANG[2], Wei-li HAN[†‡1]

[1]*The First Affiliated Hospital, College of Medicine, Zhejiang University, Hangzhou 310003, China*

[2]*Zhejiang Hospital of Traditional Chinese Medicine, Zhejiang Chinese Medical University, Hangzhou 310006, China*

[3]*Institute of Biochemistry, College of Life Sciences, Zhejiang University, Hangzhou 310058, China*

[†]E-mail: phwbhpxc@zju.edu.cn; wang.baohui888@163.com; zjhzhwldoc@zju.edu.cn

Received June 7, 2018; Revision accepted Nov. 15, 2018; Crosschecked Mar. 2, 2019

Abstract: Objective: Reactive oxygen species (ROS) are involved in a variety of biological phenomena and serve both deleterious and beneficial roles. ROS quantification and assessment of reaction networks are desirable but difficult because of their short half-life and high reactivity. Here, we describe a pro-oxidative model in a single human lung carcinoma SPC-A-1 cell that was created by application of extracellular H_2O_2 stimuli. Methods: Modified microfluidics and imaging techniques were used to determine $O_2^{\bullet-}$ levels and construct an $O_2^{\bullet-}$ reaction network. To elucidate the consequences of increased $O_2^{\bullet-}$ input, the mitochondria were given a central role in the oxidative stress mode, by manipulating mitochondria-interrelated cytosolic Ca^{2+} levels, mitochondrial Ca^{2+} uptake, auto-amplification of intracellular ROS and the intrinsic apoptotic pathway. Results and conclusions: Results from a modified microchip demonstrated that 1 mmol/L H_2O_2 induced a rapid increase in cellular $O_2^{\bullet-}$ levels (>27 vs. >406 amol in 20 min), leading to increased cellular oxidizing power (evaluated by ROS levels) and decreased reducing power (evaluated by glutathione (GSH) levels). In addition, we examined the dynamics of cytosolic Ca^{2+} and mitochondrial Ca^{2+} by confocal laser scanning microscopy and confirmed that Ca^{2+} stores in the endoplasmic reticulum were the primary source of H_2O_2-induced cytosolic Ca^{2+} bursts. It is clear that mitochondria have pivotal roles in determining how exogenous oxidative stress affects cell fate. The stress response involves the transfer of Ca^{2+} signals between organelles, ROS auto-amplification, mitochondrial dysfunction, and a caspase-dependent apoptotic pathway.

Key words: Individual cell; Superoxide anion; Reactive oxygen species (ROS) dynamics; Intrinsic apoptotic pathway; Ca^{2+} signaling

https://doi.org/10.1631/jzus.B1800319 **CLC number:** R73-3

1 Introduction

Reactive oxygen species (ROS) are chemically reactive molecules that are constantly generated and eliminated during diverse biological and cellular reactions (Thannickal and Fanburg, 2000). ROS play crucial roles in gene activation, cellular growth, and modulation of biochemical reactions (Liochev, 2013; Köhler et al., 2014). They may also function as secondary messengers in pathways, such as the Akt and

‡ Corresponding author
§ The two authors contributed equally to this work
* Project supported by the Zhejiang Provincial Natural Science Foundation of China (No. LY18H300002), the Medical Health Science and Technology Project of Zhejiang Provincial Health Commission (No. 2019RC061/2019312897), the Zhejiang Provincial Natural Science Foundation of China (Nos. Y4110212 and LY19H090001), and partly by the National Natural Science Foundation of China (Nos. 81372301 and 81301113)
ORCID: Hui PAN, https://orcid.org/0000-0002-8697-816X

mitochondria-mediated apoptosis pathways, and in the regulation of cell cycle proteins to inhibit the cell proliferation pathway (Martindale and Holbrook, 2002; Hileman et al., 2004). However, excessive ROS leakage from the mitochondria results in continuous and cumulative oxidative damage to cellular components that alter many cellular functions (Rhee, 2006; Yu et al., 2015). Increasing evidence indicates that the intrinsic ROS level of cancer cells is higher than that of normal cells, partly due to carcinogenic stimulation, metabolic activity changes, and mitochondrial dysfunction. Increased ROS levels may stimulate cell proliferation, promote mutation and genetic instability, and alter cell sensitivity to anticancer drugs. (Pelicano et al., 2004; Qin et al., 2009). These complicated roles imply that intracellular ROS levels should be tightly regulated and that appropriate ROS levels are extremely important for maintaining vital cellular and biochemical functions (Blokhina and Fagerstedt, 2010; Tang et al., 2011).

Therefore, ROS-related therapy should be designed carefully, taking into consideration their complicated roles and high reactivity. To this end, the quantitative and precise assessment of the dynamic reaction networks of ROS in live cells would be highly desirable (Labuschagne and Brenkman, 2013). A microfluidic system was developed for the analysis of single biological cells, with functional integration of cell sampling, single cell loading, docking, lysing, and capillary electrophoretic (CE) separation with laser-induced fluorescence (LIF) detection in microfabricated channels of a single glass chip (Gao et al., 2004). Microfluidic systems have become an attractive tool for the quantitative analysis of ROS in single cells, because their dimensions are comparable to those of single cells (Gao J et al., 2004; Gao N et al., 2007). In addition, imaging techniques, such as confocal laser scanning microscopy (CLSM) and fluorescence-activated cell sorting (FACS), are currently being developed for studying ROS dynamics in single cells. Studying ROS at the single-cell level will lead to a more precise determination of their behavior.

In this study, we constructed a pro-oxidative stress model within an individual SPC-A-1 tumor cell by application of exogenous H_2O_2 stimuli. Modified microfluidics and imaging techniques were used to determine $O_2^{\bullet-}$ levels and to construct an $O_2^{\bullet-}$ reaction network. To elucidate the consequences of increased $O_2^{\bullet-}$ input, the mitochondria were given a central role in the oxidative stress mode by manipulating mitochondria-interrelated cytosolic Ca^{2+} levels, mitochondrial Ca^{2+} uptake, auto-amplification of intracellular ROS and the intrinsic apoptotic pathway.

2 Materials and methods

2.1 Materials

Hydroethidine (HE), dihydrorhodamine 123 (DHR123), naphthalene-2,3-dicarboxaldehyde (NDA), and fluo-3/AM and Rhod-2/AM were obtained from Molecular Probes (Eugene, OR, USA); 3-(4,5-dimethylthiazol-2-yl)-2,5-diphenyltetrazolium bromide (MTT), trypan blue, H_2O_2, ethylene glycol-bis(β-aminoethyl ether)-*N*,*N*,*N*',*N*'-tetraacetic acid (EGTA-AM), thapsigargin (TG), and carbobenzoxy-valyl-alanyl-aspartyl-[*O*-methyl]-fluoromethylketone (z-VAD-fmk) were purchased from Sigma (St. Louis, MO, USA). Cleaved poly ADP-ribose polymerase (PARP), cytochrome *c*, B-cell lymphoma-2 (Bcl-2), Bcl-xL, Bax, Bak, and β-actin antibodies were purchased from Cell Signaling Technology (Danvers, MA, USA). All other chemicals were of the highest purity available.

The SPC-A-1 lung adenocarcinoma cell line was available in our institute and was routinely cultured in RPMI-1640 medium (Gibco, Grand Island, NY, USA) supplemented with 10% (v/v) fetal bovine serum (FBS; Gibco), 100 U/mL penicillin, and 100 U/mL streptomycin, in a humidified cell incubator at 37 °C with an atmosphere of 5% CO_2.

2.2 Construction of an oxidative stress model

The SPC-A-1 cells were washed and incubated in 1 mmol/L H_2O_2 for 10 min. After three washes, 10 μmol/L HE (special probe for $O_2^{\bullet-}$) (Lyublinskaya et al., 2014) was added for 20 min in the dark. Cells were washed, lysed, and resuspended in phosphate-buffered saline (PBS) for further measurements. Other cellular ROS (e.g. H_2O_2 and oxidative nitrogen species (ONS)) and glutathione (GSH) were also measured as above, except that the cells were simultaneously probed with 10 μmol/L DHR123 and 500 μmol/L NDA. These three non-fluorescent probes can easily penetrate the cell membrane, and are converted into fluorescent resultants (OH-E, rhodamine 123 (Rh123),

and NDA-GSH, respectively) that are non-permeant after reactions with their respective substrates ($O_2^{\bullet-}$, ROS, or GSH).

For fluorescence measurements in a single SPC-A-1 cell, a microchip was fabricated following the procedures described by Sun and Yin (2006), except that three channels were deepened: the tapered channel under a weir was 8 μm deep, and the sampling and separation channels were 37 and 15 μm deep, respectively. The cell suspension (100 μL; 1×10^5 cells/mL) was added to the microchip and electropherograms recorded fluorescence intensity. To quantify the fluorescent resultants in the SPC-A-1 cell, different concentrations of the OH-E (Zhao et al., 2003), Rh123 (Sun et al., 2005), and NDA-GSH (Gao et al., 2004) standards were prepared, and fluorescent electropherograms were recorded in the microchip.

2.3 Cell viability assay

Cell viability was measured using the MTT assay (Pan et al., 2015). Briefly, exponentially growing SPC-A-1 cells were seeded in 96-well plates. After incubating with H_2O_2 at various concentrations for the indicated time, cells were incubated with MTT for 4 h at 37 °C. Formazan precipitate was dissolved in 150 μL dimethyl sulfoxide (DMSO), and absorbance was measured at 490 nm using a Multiskan MK3 microplate reader (Thermo Fisher Scientific, Waltham, MA, USA).

Cell viability was also assessed using a trypan blue exclusion assay. Briefly, SPC-A-1 cells were cultured in 24-well plates, and then exposed to H_2O_2 at various concentrations for the indicated time. Trypan blue was added to the medium, and the percentage of viable cells was determined using a hemocytometer to count the number of cells that excluded the dye.

2.4 Cell death analysis

Apoptosis and necrosis were assessed by flow cytometry using annexin V-fluorescein isothiocyanate (V-FITC) cell apoptosis detection kit (Sigma, St. Louis, MO, USA) according to the manufacturer's instructions. Briefly, cells were cultured with H_2O_2 at various concentrations for 6 h, and 1×10^6 cells were collected and washed twice with ice-cold PBS. Early apoptotic cells (annexin V^+/PI^-) or late apoptotic/necrotic cells (annexin V^+/PI^+) were evaluated by double staining with annexin V-FITC and propidium iodide (PI) in binding buffer by flow cytometry.

To detect DNA strand breaks, a terminal deoxynucleotidyl transferase (TdT)-mediated dUTP nick-end labeling (TUNEL) assay was performed using an APO-BRDU kit (BD Biosciences, New Jersey, USA). Briefly, after incubation with H_2O_2 at various concentrations for the indicated time, cells were fixed and permeabilized with 4% paraformaldehyde and 70% ethanol, followed by incubation with a mixture of FITC-dUTP and TdT for 1 h at 37 °C. Stained cells were analyzed with flow cytometry.

An Apoptotic DNA Ladder kit (Beyotime Institute of Biotechnology) was used to analyze DNA fragmentation according to the manufacturer's instructions. DNA fragments were then separated on a 1.5% agarose gel and visualized under ultraviolet (UV) light after staining with ethidium bromide.

2.5 Cellular Ca^{2+} signal transfer

Prepared SPC-A-1 cells on glass coverslips were simultaneously loaded with Fluo-3/AM (a cytosolic Ca^{2+}-sensitive fluorescent probe) and Rhod-2/AM (a mitochondrial Ca^{2+}-sensitive fluorescent probe). Coverslips were removed and attached to a coverslip clamp chamber filled with Hank's buffer. After 60 s of basal image acquisition by CLSM, H_2O_2 was perfused into the chamber, and fluorescence images were analyzed. The final concentration of H_2O_2 was 1 mmol/L. In the D-Hank's group, probe-loaded cells were attached to the coverslip clamp chamber filled with D-Hank's buffer to remove extracellular Ca^{2+}. In the TG group, cells were pretreated with 2 μmol/L TG for 30 min to deplete Ca^{2+} stores in the endoplasmic reticulum (ER). In the EGTA-AM group, cells were pretreated with EGTA-AM using the above method to chelate free cytosolic Ca^{2+}.

2.6 ROS dynamic measurement

For dynamic measurements of $O_2^{\bullet-}$ and H_2O_2/ONS in a single cell undergoing extracellular H_2O_2 stimulation, the prepared SPC-A-1 cells on glass coverslips were loaded with dual probes (dihydroethidium (DHE), DHR123). Coverslips were removed and attached to the coverslip clamp chamber filled with Hank's buffer. After 60 s of basal image acquisition by CLSM, H_2O_2 was perfused into the chamber, and fluorescence images were analyzed.

The final concentration of H_2O_2 was 1 mmol/L. In the EGTA-AM group (depleted of free cytosolic Ca^{2+}), probe-loaded cells were pretreated with 25 μmol/L EGTA-AM for 30 min. After three washes, cells were attached to the coverslip clamp chamber, followed by H_2O_2 application.

2.7 Caspase assays

The activity of caspase-3, -8, and -9 was measured using a colorimetric assay kit (Beyotime Institute of Biotechnology, Nanjing, China) according to the manufacturer's instructions. Briefly, cell lysates from 1×10^6 cells were incubated at 37 °C for 2 h with 200 μmol/L Ac-DEVD-pNA (caspase-3 substrate), Ac-IETD-pNA (caspase-8 substrate), or Ac-LEHD-pNA (caspase-9 substrate). Samples were read at 405 nm in a Multiskan MK3 microplate reader. In the caspase inhibitor assay, cells were treated with 0–500 μmol/L H_2O_2 for 6 h, with or without 100 μmol/L z-VAD-fmk pretreatment for 2 h.

2.8 Western blot analysis

Treated cells were collected, washed in PBS, and then lysed on ice with lysis buffer. Cytosolic fractions were prepared as previously described (Qin et al., 2011). The protein concentration of each extract was determined by the Bradford assay. About 30 μg protein was separated by electrophoresis on 10% to 15% standard sodium dodecyl sulfate polyacrylamide gel electrophoresis (SDS-PAGE), and then transferred to nitrocellulose blotting membranes. Following incubation with the proper primary and secondary antibodies, proteins were visualized by chemiluminescence detection.

2.9 Statistical analysis

Data are presented as the mean±standard deviation (SD). Statistical analyses were carried out by one-way analysis of variance (ANOVA) followed by Tukey's post-hoc test. $P<0.05$ was considered to indicate a statistically significant difference.

3 Results

3.1 Construction of an oxidative stress model

The SPC-A-1 cells were treated with 1 mmol/L H_2O_2 for 10 min, followed by loading of the cells with the fluorescent probes (probes: HE, DHR123, or NDA). Relative fluorescence intensity was determined using a microfluidic chip. A typical electropherogram of OH-E in a PBS-treated SPC-A-1 cell is shown in Fig. 1a, and that of a H_2O_2-treated cell in Fig. 1b. Figs. 1c and 1d show the electropherograms of Rh123 and NDA-GSH in a PBS-treated cell and H_2O_2-treated cell, respectively. According to statistical analysis of the results from ten consecutive cells, the mean fluorescence intensities of OH-E, Rh123, and NDA-GSH in the oxidative stress model (H_2O_2-treated group) were (161.0±41.2), (74.4±18.5), and (9.0±2.6) mV·s, respectively. In the control model (PBS-treated group), the corresponding values were (20.6±6.2), (17.7±4.5), and (27.0±6.7) mV·s, respectively.

The standard curves of the three fluorescent substances are shown in Fig. 1e. Quantitative analysis showed that (84.6±25.2) amol HE, (23.2±6.0) amol DHR123, and (61.7±16.4) amol NDA were consumed by an H_2O_2-treated cell in 20 min. In the PBS-treated control group, the corresponding values were (5.7±1.3), (5.1±1.3), and (168.2±41.7) amol, respectively (Fig. 1f). We defined the value of consumed DHR123 as the cellular oxidizing power, and the value of consumed NDA as the reducing power in order to evaluate the cellular redox state. A cellular redox coordinate system was then constructed using oxidizing power as the x axis and reducing power as the y axis. Cells from the oxidative stress model showed a distinct distribution (Fig. 1g, black dots) compared to cells from the control model (Fig. 1g, triangles). Cells from the model were localized mainly in the bottom right area, while the control cells were localized mainly in the top left area. These results indicated that the oxidative stress model had been successfully constructed.

3.2 H_2O_2-induced apoptosis in SPC-A-1 cells

Cell viability was determined using an MTT assay. H_2O_2 inhibited the growth of SPC-A-1 cells in a distinct dose- and time-dependent manner. Fifty percent inhibitory concentrations (IC_{50}) were (512.4±19.2), (282.7±14.7), (172.5±11.8), and (91.9±5.6) μmol/L after incubation for 1, 3, 6, and 12 h, respectively (Fig. 2a). Trypan blue exclusion assays revealed that treatment with H_2O_2 caused a significant increase in cell death (Fig. 2b). These results were consistent with those from the MTT assay.

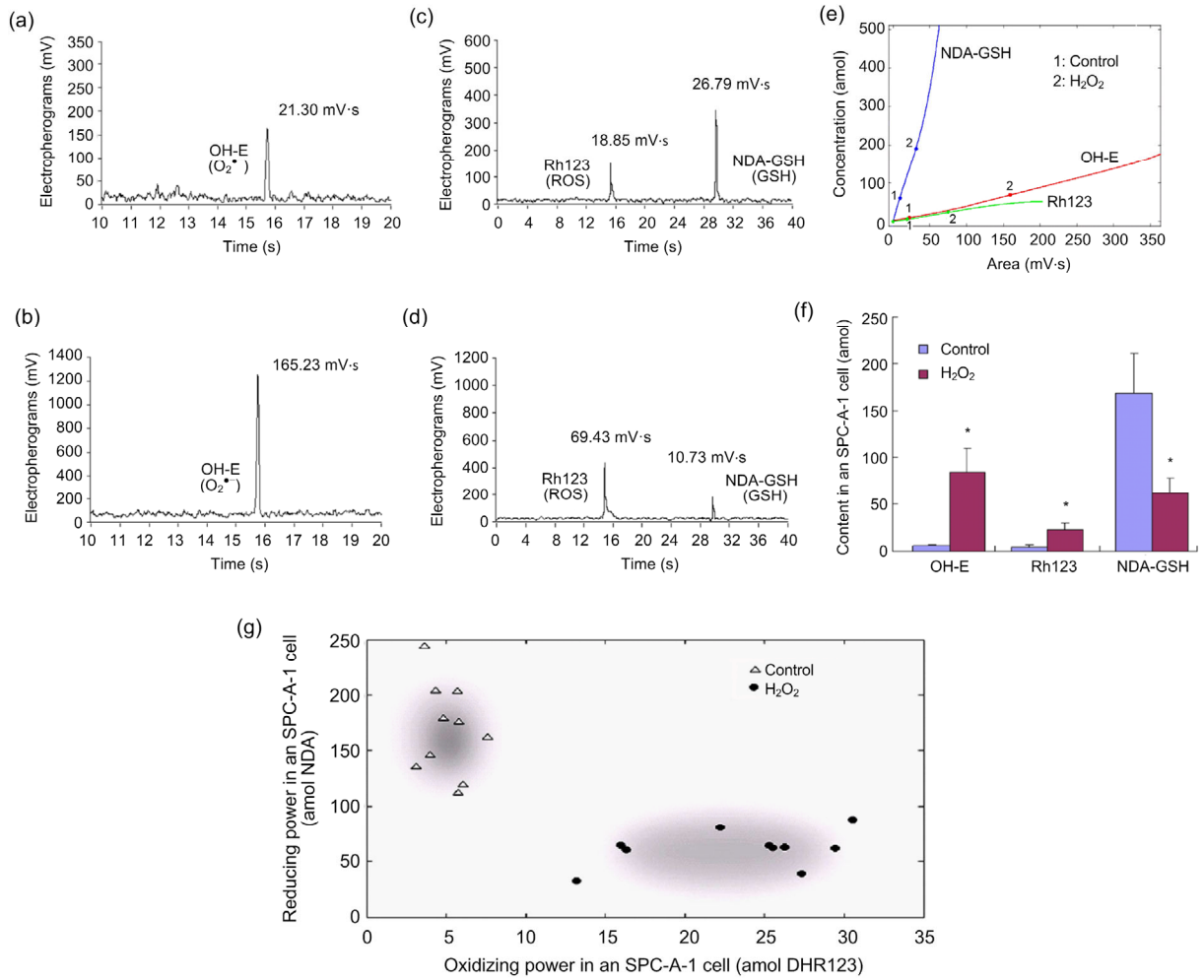

Fig. 1 Construction of the oxidative stress model

(a) A typical electropherogram of OH-E in a single SPC-A-1 cell treated with PBS. (b) A typical electropherogram of OH-E in a single SPC-A-1 cell treated with 1 mmol/L H_2O_2. (c) A typical electropherogram of Rh123 and NDA-GSH in a single SPC-A-1 cell treated with PBS. (d) A typical electropherogram of Rh123 and NDA-GSH in a single SPC-A-1 cell treated with 1 mmol/L H_2O_2. (e) Recorded areas of a series of standards of OH-E, Rh123, and NDA-GSH. (f) The average values of OH-E, Rh123, and NDA-GSH in 10 SPC-A-1 cells from microchip analysis. The values of fluorescence resultants were determined by comparison to standards of OH-E, Rh123, and NDA-GSH ($^*P$<0.05 vs. PBS control). (g) Redox coordinate system of SPC-A-1 cells. The oxidizing power (value of consumed DHR123/cell) as the *x* axis and the reducing power (value of consumed NDA/cell) as the *y* axis were used to construct a cellular redox coordinate system

In the TUNEL assay, flow-cytometric analysis showed that H_2O_2 treatment of SPC-A-1 cells caused a dose- and time-dependent increase in the percentage of apoptotic cells (TUNEL-positive cells). Compared to the controls, cells treated with 200 μmol/L H_2O_2 for 6 h had a distinct increase in the percentage of apoptotic cells from 1.41% to 44.37% (Figs. 2c and 2d). Compared to the control, following treatment with 200 μmol/L H_2O_2, the percentage of early apoptotic cells (annexin V^+/PI^-) increased from 1.37% to 38.76%, and the percentage of late apoptotic/necrotic cells (annexin V^+/PI^+) increased from 1.52% to 16.49%. Further evidence for an increase in apoptosis was the distinct rise in the percentage of late apoptotic/necrotic cells, which was apparent at a concentration of 500 μmol/L (Fig. 2e). In addition, the genomic DNA of cells treated with 200 μmol/L H_2O_2 for 6 h showed typical DNA fragment ladders (Fig. 2f). These results demonstrated that apoptosis was the main cause of decreased cell viability in H_2O_2-treated cells.

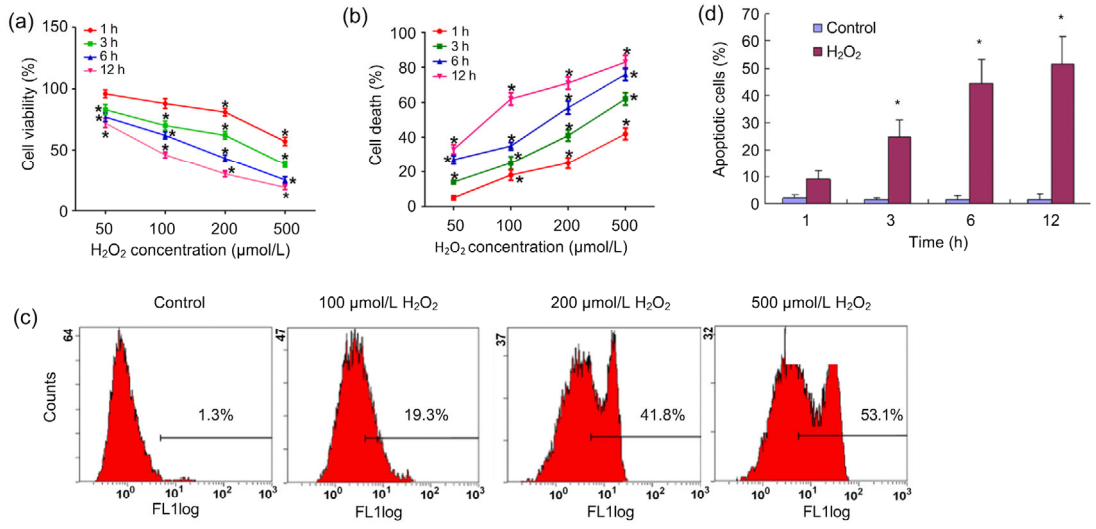

(e)

H_2O_2 (μmol/L)	Apoptotic cells (%)			
	Annexin V^-/PI^+	Annexin V^+/PI^+	Annexin V^-/PI^-	Annexin V^+/PI^-
0	0.19±0.08	1.52±0.36	96.92±0.68	1.37±0.42
100	0.46±0.04	9.84±1.45	71.03±3.48	18.67±2.12
200	2.13±0.56	16.49±1.25	42.62±3.27	38.76±2.21
200	4.52±1.25	55.32±5.28	18.68±2.62	21.48±1.85

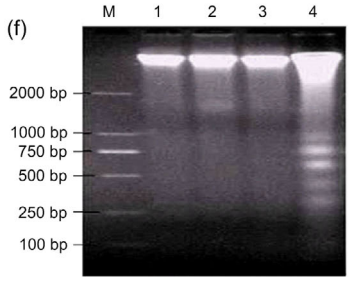

Fig. 2 Dose- and time-dependent cytotoxicity of H_2O_2 in SPC-A-1 cells

(a) H_2O_2 induced a decrease in cell viability in the SPC-A-1 cell, as determined with the MTT assay. (b) Trypan blue exclusion assays revealed that treatment with H_2O_2 caused a significant increase in cell death. (c) SPC-A-1 cells were treated with 0–500 μmol/L H_2O_2 for 6 h, and then apoptosis was determined by the TUNEL assay. Data represent similar results from three independent experiments. (d) SPC-A-1 cells were treated with 200 μmol/L H_2O_2 for 1–12 h, and then apoptosis was determined by the TUNEL assay. (e) SPC-A-1 cells were treated with 0–500 μmol/L H_2O_2 for 6 h, and then early apoptotic cells (annexin V^+/PI^-) or late apoptotic and necrotic cells (annexin V^+/PI^+) were identified by flow cytometry analysis using an annexin V-FITC/PI staining kit. The number of apoptotic cells in each apoptotic stage is expressed as a percentage of the total number of cells. (f) Effect of H_2O_2 on DNA fragmentation in SPC-A-1 cells. M: DNA ladder; Lanes 1−4 represent 200 μmol/L H_2O_2 for 0, 1, 3, and 6 h, respectively. Data represent the mean±SD of three independent experiments ($^*P<0.05$ vs. PBS control)

3.3 H_2O_2-induced cellular Ca^{2+} signal transfer and intracellular ROS dynamic increase

Cytosolic Ca^{2+} and mitochondrial Ca^{2+} were visualized instantaneously, and semi-quantification of the fluorescence was achieved by CLSM. Exposure to 1 mmol/L H_2O_2 induced a distinct increase in green fluorescence (>4.5-fold) and red fluorescence (>2-fold) in 60–180 s, reflecting increased cytosolic Ca^{2+} and mitochondrial Ca^{2+} levels (Fig. 3a). Fluorescence levels became relatively steady after 240 s.

To probe the origin of the cytosolic Ca^{2+} bursts, the ER Ca^{2+} store was depleted by TG. In this case, the burst of cytosolic Ca^{2+} was largely inhibited, suggesting that the ER Ca^{2+} store was the primary and earlier origin of cytosolic Ca^{2+}. In addition, the removal of extracellular Ca^{2+} also slightly alleviated the increase of cytosolic Ca^{2+} (in the D-Hank's group), implying that the influx of external Ca^{2+} also contributed, to some extent, to cytosolic Ca^{2+} overload. It is generally recognized that a burst of cytosolic Ca^{2+} will lead to an overload of mitochondrial Ca^{2+}. To confirm this in H_2O_2-treated cells, free cytosolic Ca^{2+} was eliminated by EGTA-AM treatment. Notably, EGTA-AM did not completely abolish the overload of mitochondrial Ca^{2+}, revealing that there was another source of overloaded mitochondrial Ca^{2+}, aside from free cytosolic Ca^{2+}.

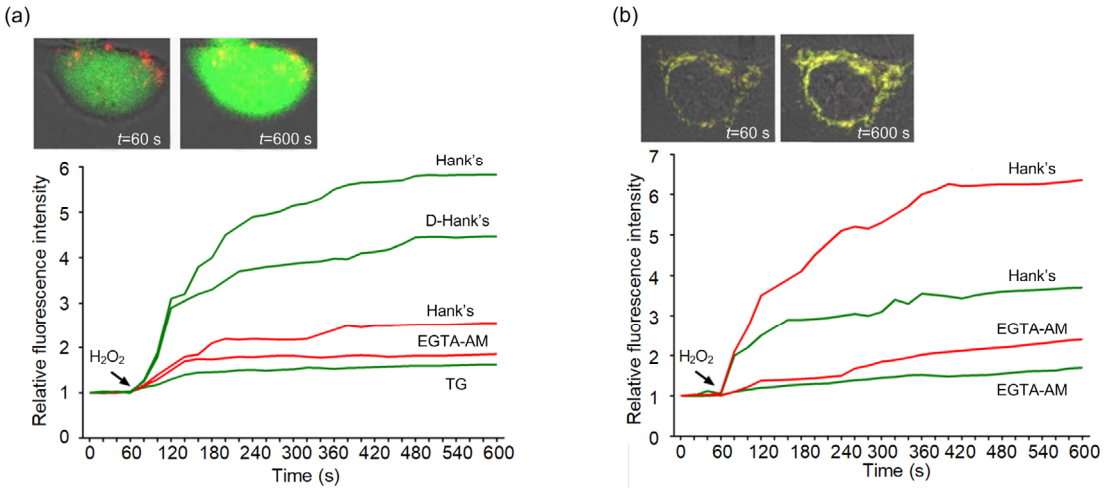

Fig. 3 Cytosolic Ca^{2+}, mitochondrial Ca^{2+}, and cellular ROS dynamics under stimulus of exogenous H_2O_2 in SPC-A-1 cells

(a) Prepared SPC-A-1 cells were loaded with Fluo-3 (green line, cytosolic Ca^{2+}) and Rhod-2 (red line, mitochondrial Ca^{2+}) and placed in Hank's buffer for CLSM observation. After 60 s, H_2O_2 was perfused into the chamber. Thirty confocal fluorescent images were taken from 1 to 600 s. The two images above show the Ca^{2+} fluorescence responses to 1 mmol/L H_2O_2 exposure in a region of interest (ROI; time (*t*)=60 s, *t*=600 s). (b) Prepared SPC-A-1 cells were loaded with HE (for $O_2^{\bullet-}$, red line) and DHR123 (for H_2O_2/ONS, green line) for CLSM observation. After 60 s of observation, 1 mmol/L H_2O_2 was added. Thirty confocal fluorescent images were taken from 1 to 600 s. The acquisition rate was 1 frame per 20 s. The obtained images were semi-quantitatively analyzed for changes in fluorescence intensities within an ROI (*n*=20) using Zeiss LSM510 software. The two images above show ROS fluorescence ($O_2^{\bullet-}$ and H_2O_2) responses to 1 mmol/L H_2O_2 exposure in an ROI (*t*=60 s, *t*=600 s). Results are expressed as the ratio of relative fluorescence intensity (100% of fluorescence intensity at 1 s). In the EGTA-AM control group, cells were pretreated with EGTA-AM to remove free cytosolic Ca^{2+} (Note: for interpretation of the references to color in this figure legend, the reader is referred to the web version of this article)

Exposure to 1 mmol/L H_2O_2 induced a marked increase in red fluorescence intensity (HE, red line, >6-fold) and green fluorescence intensity (DHR123, green line, Hank's control, >4-fold) (Fig. 3b). Although fluorescence intensity from image analysis does not represent the actual concentrations of $O_2^{\bullet-}$ and H_2O_2/ONS, it indicates that $O_2^{\bullet-}$ and H_2O_2/ONS levels increased. This was consistent with the results from microchip analysis. However, after free cytosolic Ca^{2+} was chelated by pretreatment with EGTA-AM (a cell permeable intracellular Ca^{2+} chelator), the increase in both HE and DHR123 fluorescence induced by H_2O_2 was observably attenuated, implying that the cellular Ca^{2+} signal was indispensable for the H_2O_2-induced ROS burst.

3.4 Mediation of H_2O_2-induced apoptosis through an intrinsic pathway

We examined the activity of caspase-3, -8, and -9 by colorimetric analysis. Although there was little increase in the activity of caspase-8, H_2O_2 treatment increased the activity of caspase-9 and caspase-3 in a dose-dependent manner compared to PBS-treated cells (Fig. 4a). In addition, pretreatment of SPC-A-1 cells with 100 μmol/L z-VAD-fmk resulted in a significant inhibition of H_2O_2-induced apoptosis (Fig. 4b), indicating that the decreased cell viability in H_2O_2-treated cells is dependent upon caspases. Incubation of SPC-A-1 cells with H_2O_2 resulted in the appearance of the 85-kDa PARP cleavage product in a dose-dependent manner (Fig. 4c). Caspase activity and PARP cleavage are intracellular indicators of activation of the apoptotic machinery. Together, these data demonstrate that H_2O_2 induces cytotoxicity of SPC-A-1 cells through an apoptotic mechanism, dependent upon caspase activation.

These results indicate that H_2O_2-induced apoptosis was most likely to occur through intrinsic pathways. To further determine the mitochondrial involvement in H_2O_2-mediated apoptotic cell death, we examined the release of mitochondrial cytochrome *c* from mitochondria into the cytoplasm. Western blot analysis showed that the relative content of cytochrome *c* in the cytosol treated with H_2O_2

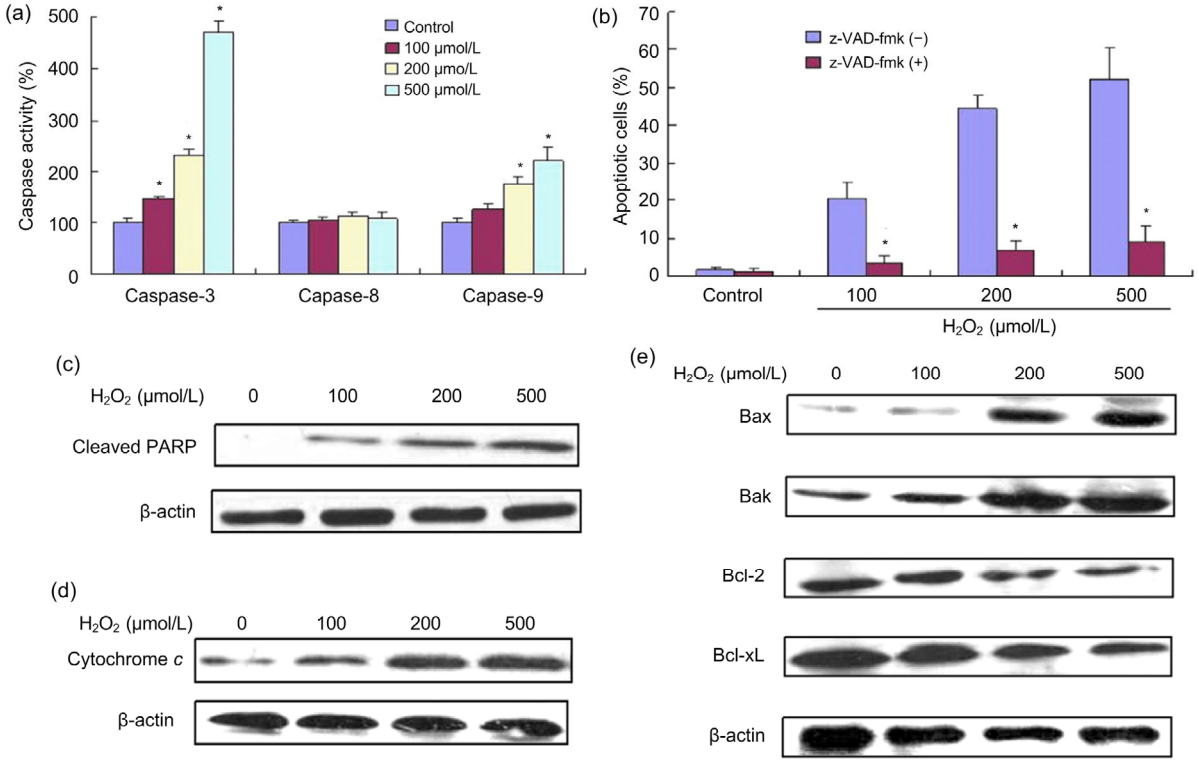

Fig. 4 Mediation of H_2O_2-induced apoptosis through the mitochondrial pathway in SPC-A-1 cells

(a) Involvement of caspase activation in H_2O_2-induced apoptosis. After treatment with 0–500 μmol/L H_2O_2 for 6 h, the cytosolic fraction of cells was analyzed for changes in caspase-3, -8, and -9 activity using a colorimetric assay. * P<0.05, vs. PBS control. (b) SPC-A-1 cells were treated with 0–500 μmol/L H_2O_2 for 6 h, with (+) or without (−) 100 μmol/L z-VAD-fmk pretreatment for 2 h, and then apoptosis was determined by the TUNEL assay. * P<0.05, vs. z-VAD-fmk (−). (c) Dose response of cleaved-PARP by H_2O_2 in SPC-A-1 cells. After treatment with H_2O_2 for 6 h, cells were disrupted, and the cellular cleaved-PARP and β-actin levels were analyzed by western blotting. (d) Dose response of cytochrome *c* by H_2O_2 in SPC-A-1 cells. After treatment with H_2O_2 for 6 h, cells were disrupted, the cytosolic fraction was isolated, and the content of cytochrome *c* was examined by western blotting analysis. (e) Dose responses of pro-apoptotic and anti-apoptotic proteins to H_2O_2 in SPC-A-1 cells. After treatment with H_2O_2 for 6 h, cells were disrupted, and cellular Bcl-2, Bcl-xL, Bax, Bak, and β-actin levels were analyzed by western blotting. Data represent the mean±SD of three independent experiments

increased significantly in a dose-dependent manner (Fig. 4d).

To confirm whether the apoptosis of SPC-A-1 cells induced by H_2O_2 is related to pro-apoptotic and anti-apoptotic regulatory proteins, we analyzed the expression of Bcl-2 family members and inhibitors of apoptotic proteins by western blotting. H_2O_2 down-regulated the expression of Bcl-2 and Bcl-xL (anti-apoptotic regulatory proteins) and enhanced the expression of Bax and Bak (pro-apoptotic regulatory proteins) in a dose-dependent manner (Fig. 4e). These observations indicate that H_2O_2-induced apoptosis in SPC-A-1 cells is mediated through an intrinsic pathway.

4 Discussion

An estimation of intracellular ROS production in an individual and intact tumor cell would be highly desirable, but remains a challenge. The relatively high reproducibility, low detection limits of microchips, and subsequent dynamic semi-quantified verification contributed to the reliability of the current single-cell study. We found, for the first time, that an SPC-A-1 tumor cell could generally consume about 5.7 amol HE in 20 min.

It is estimated that 1%–2% of the electron flow in the mitochondria normally leaks from the electron transport chain to form $O_2^{\bullet-}$. The most important

metabolic reaction of cellular $O_2^{\bullet-}$ is dismutation and the formation of other ROS (H_2O_2 and ONS). Other ROS can be eliminated through GSH reduction (Maltepe and Saugstad, 2009; von Montfort et al., 2012). These reactions showed the origin and main fate of $O_2^{\bullet-}$. As the output of $O_2^{\bullet-}$ was evaluated in the above discussions, we further evaluated other ROS and GSH. As lower specialties of DHR123 and NDA, we did not estimate the precise outputs or inputs; here we just defined the values of consumed DHR123 and NDA as the cellular oxidizing power and cellular reducing power, respectively. A typical SPC-A-1 cell exhibits 5 amol oxidizing power and 168 amol reducing power (Fig. 1g). A 1 mmol/L H_2O_2-induced $O_2^{\bullet-}$ burst (>27 vs. >406 amol) led to a significant increase in cellular oxidizing power (5 vs. 23 amol). Subsequently, the increased oxidizing power consumed limited GSH (168 vs. 62 amol) in the cellular environment. In all, oxidizing and reducing powers interacted with each other, as shown by the two distinctive dot distributions in Fig. 1g.

The relationship between Ca^{2+} and oxidative stress has been extensively studied. It has been reported that the synthesis of calcium-activated reductive substrates (NADH) and the acceleration of electron transfer chain increase ROS production (Voronina et al., 2002; Spät and Pitter, 2004; Camello-Almaraz et al., 2006). Conversely, high ROS levels facilitate Ca^{2+} accumulation by promoting release from internal stores and damaging Ca^{2+} scavenging systems (Feng et al., 2000). Ca^{2+}/ROS positive feedback has been confirmed in previous studies (Singh et al., 2005; Tonks, 2005). As a consequence of Ca^{2+} uptake, mitochondria can suffer Ca^{2+} overload, triggering the opening of the permeability transition pore (PTP), which is associated with apoptosis via the mitochondrial pathway or necrosis due to mitochondrial damage (Moreau et al., 2006; Akopova, 2008). Although oxidative stress is usually associated with cellular Ca^{2+} signals (Mota et al., 2015; Orrenius et al., 2015), a precise Ca^{2+} signaling transfer pathway is relatively obscure. In our oxidative stress model, oxidative stress stimuli led to rapid and significant increases in free cytosolic Ca^{2+}, which were largely abolished by depletion of ER Ca^{2+}, strongly suggesting that the ER Ca^{2+} store was the primary source of increased free Ca^{2+}. It seems that the origin of cytosolic Ca^{2+} bursts under oxidative-pathological conditions (ER) differs from that under oxidative-physiological conditions (extracellular circumstance) (Yuana et al., 2013). Extracellular Ca^{2+} also contributed slightly to cytosolic Ca^{2+} bursts. However, it remains to be investigated how the exogenous H_2O_2 signal traverses the membrane to access the cytoplasm. As a relatively important cellular Ca^{2+} store, mitochondria can stabilize intracellular Ca^{2+} levels by uptake or release of cytosolic Ca^{2+}. In the present study, mitochondrial Ca^{2+} was significantly overloaded in the oxidative model. Application of EGTA-AM (to eliminate cytosolic free Ca^{2+}) could not completely abolish this overload. This suggests that free cytosolic Ca^{2+} may not be the only origin of the overloaded mitochondrial Ca^{2+}. The overload might also be attributable to the channels that directly connect the ER to mitochondria (de Marchi et al., 2014; Giorgi et al., 2015).

Ca^{2+}/ROS positive feedback has been proven in previous studies (Singh et al., 2005; Bogeski et al., 2011). We considered that the mitochondria may be the main origin of ROS bursts in the current model (but not H_2O_2, after permeating the cell membrane) for the following reasons. Firstly, $O_2^{\bullet-}$ levels increased significantly during oxidative stimuli. As a progenitor of other ROS (involving H_2O_2), it is impossible to produce $O_2^{\bullet-}$ by direct conversion of exogenous H_2O_2. $O_2^{\bullet-}$ can be produced only through mitochondrial electron leakage. Secondly, increased $O_2^{\bullet-}$ and H_2O_2 fluorescence was localized mostly in the mitochondria (Fig. 3a). However, when exogenous H_2O_2 was increased to 50 mmol/L (this stimulus was believed to be considerably destructive to the cell membrane), H_2O_2 fluorescence was quite uniformly distributed in the cytoplasm. In this case, exogenous H_2O_2 destroyed and permeated the cell membrane, contributing much to the increased cellular H_2O_2 levels. These observations indicate that H_2O_2-induced ROS bursts were derived from the mitochondria. As noted by Rhee (2006), cell membranes are poorly permeable to H_2O_2.

In the oxidative model, Bax and Bak were markedly up-regulated whereas Bcl-2 and Bcl-xL were down-regulated. This led to the subsequent release of cytochrome *c* from the mitochondria. The increase in the activity of caspase-9 in H_2O_2-treated

SPC-A-1 cells also indicated that H_2O_2-induced apoptosis was most likely to occur through the mitochondrial pathway. Caspase-3 is required for DNA fragmentation and morphological alterations associated with apoptosis (Solier and Pommier, 2011). In our oxidative model, we observed that the release of cytochrome *c* from the mitochondria resulted in an increase in the activity of caspase-9 in H_2O_2-treated SPC-A-1 cells, subsequently leading to an increase in caspase-3 activity.

In conclusion, our research has shown that 1 mmol/L H_2O_2 induces a rapid increase in cellular $O_2^{\bullet-}$ levels (>27 vs. >406 amol, in 20 min), leading to increased cellular oxidizing power and decreased reducing power. In addition, our results clearly demonstrate that increased oxidative stress modulates the dynamics of Ca^{2+} release, allowing for an explosive efflux of cytosolic Ca^{2+} from internal stores (ER), and concomitant mitochondrial Ca^{2+} uptake. The mitochondria appear to have a central role in determining how exogenous oxidative stress affects cell fate. The mechanism involves endogenous ROS auto-amplification, regulation of pro-apoptotic and anti-apoptotic proteins, cytochrome *c* release, and increases in caspase activity.

Contributors

Hui PAN designed the project and performed data analysis. Bao-hui WANG carried out data processing, performed data analysis, and wrote the paper. Zhou-bin LI contributed to western blotting analysis. Xing-guo GONG and Yong QIN contributed to ROS dynamic measurement. Yan JIANG contributed to the TUNEL assay. Wei-li HAN contributed to the paper writing and the design of the project. All authors read and approved the final manuscript. Therefore, all authors have full access to all the data in the study and take responsibility for the integrity and security of the data.

Compliance with ethics guidelines

Hui PAN, Bao-hui WANG, Zhou-bin LI, Xing-guo GONG, Yong QIN, Yan JIANG, and Wei-li HAN declare that they have no conflict of interest.

This article does not contain any studies with human or animal subjects performed by any of the authors.

References

Akopova OV, 2008. The role of mitochondrial permeability transition pore in transmembrane Ca^{2+}-exchange in mitochondria. *Ukr Biokhim Zh (1999)*, 80(3):40-47 (in Ukrainian).

Blokhina O, Fagerstedt KV, 2010. Oxidative metabolism, ROS and NO under oxygen deprivation. *Plant Physiol Biochem*, 48(5):359-373. https://doi.org/10.1016/j.plaphy.2010.01.007

Bogeski I, Kappl R, Kummerow C, et al., 2011. Redox regulation of calcium ion channels: chemical and physiological aspects. *Cell Calcium*, 50(5):407-423. https://doi.org/10.1016/j.ceca.2011.07.006

Camello-Almaraz C, Gomez-Pinilla PJ, Pozo MJ, et al., 2006. Mitochondrial reactive oxygen species and Ca^{2+} signaling. *Am J Physiol Cell Physiol*, 291(5):C1082-C1088. https://doi.org/10.1152/ajpcell.00217.2006

de Marchi E, Bonora M, Giorgi C, et al., 2014. The mitochondrial permeability transition pore is a dispensable element for mitochondrial calcium efflux. *Cell Calcium*, 56(1):1-13. https://doi.org/10.1016/j.ceca.2014.03.004

Feng W, Liu GH, Allen PD, et al., 2000. Transmembrane redox sensor of ryanodine receptor complex. *J Biol Chem*, 275(46):35902-35907. https://doi.org/10.1074/jbc.C000523200

Gao J, Yin XF, Fang ZL, 2004. Integration of single cell injection, cell lysis, separation and detection of intracellular constituents on a microfluidic chip. *Lab Chip*, 4(1):47-52. https://doi.org/10.1039/b310552k

Gao N, Li L, Shi ZK, et al., 2007. High-throughput determination of glutathione and reactive oxygen species in single cells based on fluorescence images in a microchannel. *Electrophoresis*, 28(21):3966-3975. https://doi.org/10.1002/elps.200700124

Giorgi C, Missiroli S, Patergnani S, et al., 2015. Mitochondria-associated membranes: composition, molecular mechanisms, and physiopathological implications. *Antioxid Redox Signal*, 22(12):995-1019. https://doi.org/10.1089/ars.2014.6223

Hileman EO, Liu JS, Albitar M, et al., 2004. Intrinsic oxidative stress in cancer cells: a biochemical basis for therapeutic selectivity. *Cancer Chemother Pharmacol*, 53(3):209-219. https://doi.org/10.1007/s00280-003-0726-5

Köhler AC, Sag CM, Maier LS, 2014. Reactive oxygen species and excitation-contraction coupling in the context of cardiac pathology. *J Mol Cell Cardiol*, 73:92-102. https://doi.org/10.1016/j.yjmcc.2014.03.001

Labuschagne CF, Brenkman AB, 2013. Current methods in quantifying ROS and oxidative damage in *Caenorhabditis elegans* and other model organism of aging. *Ageing Res Rev*, 12(4):918-930. https://doi.org/10.1016/j.arr.2013.09.003

Liochev SI, 2013. Reactive oxygen species and the free radical theory of aging. *Free Radic Biol Med*, 60:1-4. https://doi.org/10.1016/j.freeradbiomed.2013.02.011

Lyublinskaya OG, Zenin VV, Shatrova AN, et al., 2014. Intracellular oxidation of hydroethidine: compartmentalization and cytotoxicity of oxidation products. *Free Radic Biol Med*, 75:60-68. https://doi.org/10.1016/j.freeradbiomed.2014.07.008

Maltepe E, Saugstad OD, 2009. Oxygen in health and disease: regulation of oxygen homeostasis-clinical implications. *Pediatr Res*, 65(3):261-268. https://doi.org/10.1203/PDR.0b013e31818fc83f

Martindale JL, Holbrook NJ, 2002. Cellular response to oxidative stress: signaling for suicide and survival. *J Cell Physiol*, 192(1):1-15. https://doi.org/10.1002/jcp.10119

Moreau B, Nelson C, Parekh AB, 2006. Biphasic regulation of mitochondrial Ca^{2+} uptake by cytosolic Ca^{2+} concentration. *Curr Biol*, 16(16):1672-1677. https://doi.org/10.1016/j.cub.2006.06.059

Mota SI, Costa RO, Ferreira IL, et al., 2015. Oxidative stress involving changes in Nrf2 and ER stress in early stages of Alzheimer's disease. *Biochim Biophys Acta*, 1852(7):1428-1441. https://doi.org/10.1016/j.bbadis.2015.03.015

Orrenius S, Gogvadze V, Zhivotovsky B, 2015. Calcium and mitochondria in the regulation of cell death. *Biochem Biophys Res Commun*, 460(1):72-81. https://doi.org/10.1016/j.bbrc.2015.01.137

Pan H, Wang BH, Lv W, et al., 2015. Esculetin induces apoptosis in human gastric cancer cells through a cyclophilin D-mediated mitochondrial permeability transition pore associated with ROS. *Chemico-Biological Interactions*, 242:51-60. https://doi.org/10.1016/j.cbi.2015.09.015

Pelicano H, Carney D, Huang P, 2004. ROS stress in cancer cells and therapeutic implications. *Drug Resist Updat*, 7(2):97-110. https://doi.org/10.1016/j.drup.2004.01.004

Qin Y, Chen FD, Zhou L, et al., 2009. Proliferative and antiproliferative effects of thymosin α1 on cells are associated with manipulation of cellular ROS levels. *Chem Biol Interact*, 180(3):383-388. https://doi.org/10.1016/j.cbi.2009.05.006

Qin Y, Pan X, Tang TT, et al., 2011. Anti-proliferative effects of the novel squamosamide derivative (FLZ) on HepG2 human hepatoma cells by regulating the cell cycle-related proteins are associated with decreased Ca^{2+}/ROS levels. *Chem Biol Interact*, 193(3):246-253. https://doi.org/10.1016/j.cbi.2011.07.004

Rhee SG, 2006. Cell signaling: H_2O_2, a necessary evil for cell signaling. *Science*, 312(5782):1882-1883. https://doi.org/10.1126/science.1130481

Singh DK, Kumar D, Siddiqui Z, et al., 2005. The strength of receptor signaling is centrally controlled through a cooperative loop between Ca^{2+} and an oxidant signal. *Cell*, 121(2):281-293. https://doi.org/10.1016/j.cell.2005.02.036

Solier S, Pommier Y, 2011. MDC1 cleavage by caspase-3: a novel mechanism for inactivating the DNA damage response during apoptosis. *Cancer Res*, 71(3):906-913. https://doi.org/10.1158/0008-5472.CAN-10-3297

Spät A, Pitter JG, 2004. The effect of cytoplasmic Ca^{2+} signal on the redox state of mitochondrial pyridine nucleotides. *Mol Cell Endocrinol*, 215(1-2):115-118. https://doi.org/10.1016/j.mce.2003.11.004

Sun Y, Yin XF, 2006. Novel multi-depth microfluidic chip for single cell analysis. *J Chromatogr A*, 1117(2):228-233. https://doi.org/10.1016/j.chroma.2006.03.088

Sun Y, Yin XF, Ling YY, et al., 2005. Determination of reactive oxygen species in single human erythrocytes using microfluidic chip electrophoresis. *Anal Bioanal Chem*, 382(7):1472-1476. https://doi.org/10.1007/s00216-005-3352-8

Tang HY, Qin Y, Li JY, et al., 2011. The scavenging of superoxide radicals promotes apoptosis induced by a novel cell-permeable fusion protein, sTRAIL:FeSOD, in tumor necrosis factor-related apoptosis-inducing ligand-resistant leukemia cells. *BMC Biol*, 9:18. https://doi.org/10.1186/1741-7007-9-18

Thannickal VJ, Fanburg BL, 2000. Reactive oxygen species in cell signaling. *Am J Physiol Lung Cell Mol Physiol*, 279(6):L1005-L1028. https://doi.org/10.1152/ajplung.2000.279.6.L1005

Tonks NK, 2005. Redox redux: revisiting PTPs and the control of cell signaling. *Cell*, 121(5):667-670. https://doi.org/10.1016/j.cell.2005.05.016

von Montfort C, Matias N, Fernandez A, et al., 2012. Mitochondrial GSH determines the toxic or therapeutic potential of superoxide scavenging in steatohepatitis. *J Hepatol*, 57(4):852-859. https://doi.org/10.1016/j.jhep.2012.05.024

Voronina S, Sukhomlin T, Johnson PR, et al., 2002. Correlation of NADH and Ca^{2+} signals in mouse pancreatic acinar cells. *J Physiol*, 539:41-52. https://doi.org/10.1113/jphysiol.2001.013134

Yu SY, Jang Y, Paik D, et al., 2015. *Nmdmc* overexpression extends *Drosophila* lifespan and reduces levels of mitochondrial reactive oxygen species. *Biochem Biophys Res Commun*, 465(4):845-850. https://doi.org/10.1016/j.bbrc.2015.08.098

Yuana Y, Sturk A, Nieuwland R, 2013. Extracellular vesicles in physiological and pathological conditions. *Blood Rev*, 27(1):31-39. https://doi.org/10.1016/j.blre.2012.12.002

Zhao HT, Kalivendi S, Zhang H, et al., 2003. Superoxide reacts with hydroethidine but forms a fluorescent product that is distinctly different from ethidium: potential implications in intracellular fluorescence detection of superoxide. *Free Radic Biol Med*, 34(11):1359-1368. https://doi.org/10.1016/S0891-5849(03)00142-4

中文概要

题　目：外源性氧化应激诱导的线粒体超氧阴离子决定肿瘤细胞命运：一项基于单个细胞的研究

目　的：通过细胞外过氧化氢（H_2O_2）的刺激建立单个人肺癌 SPC-A-1 细胞的氧化压力模型。

创新点：氧自由基（ROS）涉及多种生物现象，包括有益和有害两个方面。ROS 的定量检测和反应网络的评估结果令人期待。但 ROS 半衰期很短且反应过程很快，因此，我们通过多种手段克服了检测和评估的困难。

方　法：利用改进的微流控和成像技术测定 ROS 水平，构建氧反应网络。通过调控线粒体胞浆 Ca^{2+}水平、线粒体 Ca^{2+}摄取、细胞内 ROS 自扩增以及内在凋亡途径，确定线粒体在外源氧化压力模式中扮演的角色。

结　论：研究结果表明 1 mmol/L H_2O_2 引起细胞 $O_2^{\bullet-}$水平的快速增加，从而导致细胞氧化能力增加和还原能力降低。此外，研究还证实了内质网中储存的 Ca^{2+}是 H_2O_2 诱导的线粒体 Ca^{2+}爆发的主要来源。外源氧化压力反应涉及细胞器间 Ca^{2+}信号的传递、ROS 自身扩增、线粒体功能紊乱和半胱天冬酶依赖性凋亡途径。线粒体在外源性氧化应激影响细胞命运方面发挥着关键作用。

关键词：单个细胞；超氧阴离子；氧自由基动力学；内源性凋亡途径；钙信号